Emergent Structural Mechanisms for High-Density Collective Motion Inspired by Human Crowds

Arianna Bottinelli,[1,*] David T. J. Sumpter,[1,†] and Jesse L. Silverberg[2,‡]
[1]Mathematics Department, Uppsala University, Lägerhyddsvägen 1, Uppsala 75106, Sweden
[2]Wyss Institute for Biologically Inspired Engineering, Harvard University, Boston, Massachusetts 02115, USA
(Received 29 June 2016; revised manuscript received 19 September 2016; published 23 November 2016)

Collective motion of large human crowds often depends on their density. In extreme cases like heavy metal concerts and black Friday sales events, motion is dominated by physical interactions instead of conventional social norms. Here, we study an active matter model inspired by situations when large groups of people gather at a point of common interest. Our analysis takes an approach developed for jammed granular media and identifies Goldstone modes, soft spots, and stochastic resonance as structurally driven mechanisms for potentially dangerous emergent collective motion.

DOI: 10.1103/PhysRevLett.117.228301

Studies of collective motion cover a broad range of systems including humans, fish, birds, locusts, cells, vibrated rice, colloids, actin-myosin networks, and even robots [1–3]. Often, theoretical models of these active matter systems take a Newtonian approach by calculating individual trajectories generated *in silico* from the sum of forces acting on each of N particles [3]. Of the work focusing on humans, social interactions such as collision avoidance, tendencies to stay near social in-group members, directional alignment, and preference for personal space have been examined to understand their role in emergent behavior [4–7]. Generally, these studies show order-disorder transitions are driven by the competition between social interactions and randomizing forces [8,9]. Models based on these findings have been incorporated into predictive tools used to enhance crowd management strategies at major organized gatherings; however, the validity of this approach is diminished in extreme social situations such as riots, protests, and escape panic [10–12]. In these situations, conventional social interactions no longer apply [13], and the actual collective behavior can be quite different from model predictions [14,15].

Situations involving large groups of people packed at high densities provide a unique view of emergent collective behavior in extreme conditions [8,10]. For example, attendees at heavy metal concerts often try to get as close as possible to the stage but are unable to do so due to the sheer number of people trying to attain the same goal [Fig. 1(a)]. Consequently, the audience in this region of the concert venue becomes a densely packed shoulder-to-shoulder group with little room for individuals to freely move. Often, the stresses involved become dangerously high and security professionals standing behind physical barriers are required to pull audience members from the crowd for medical attention [16]. At black Friday sales events, we find similar situations when individuals seeking low-cost consumer goods congregate at the entrance of a store before it opens [Fig. 1(b)]. As documented in many reports and online videos, these events can have tragic outcomes in the critical moments after the doors open and the crowd surges forward resulting in stampedes and trampling.

In extreme situations involving large high-density crowds, physical interactions between contacting bodies and the simultaneous collective desire of each individual to get to a stage, through a door, or to a particular location become the dominant considerations [5,12,17]. To generically capture these scenarios, we use a conventional force-based active matter model for human collective motion, but remove terms that account for social interaction. With this simplification, we have an *asocial* model for human collective behavior describing people aggregating around a common point of interest $\mathcal{P}$. Here, we place $\mathcal{P}$ at the side of a 2D $L \times L$ simulation box [Fig. 1(c)]. In this framework, each person i is modeled as a disk with radius $r_0 \ll L$ positioned at a point $\vec{r}_i(t)$ and subject to pairwise collision forces $\vec{F}_i^{\text{repulsion}}$, a self-propulsion force $\vec{F}_i^{\text{propulsion}}$, random force fluctuations from environmental stimuli $\vec{F}_i^{\text{noise}}$, and a rigid-wall collision force $\vec{F}_i^{\text{wall}}$.

For each of the N self-propelled particles (SPPs) in our model we have $\vec{F}_i^{\text{repulsion}} = \epsilon \sum_{j \neq i}^{N} (1 - r_{ij}/2r_0)^{3/2} \hat{r}_{ij}$, which takes nonzero values only when the distance between two particles $|\vec{r}_i - \vec{r}_j| = |r_{ij}\hat{r}_{ij}| = r_{ij} < 2r_0$ [8]: $\vec{F}_i^{\text{propulsion}} = \mu(v_0 - v_i)\hat{p}_i$, where v_0 is a constant preferred speed, v_i is the current speed of the ith SPP, and $\hat{p}_i$ is a unit vector pointing from each particle's center to the common point of interest $\mathcal{P}$; $\vec{F}_i^{\text{noise}} = \vec{\eta}_i$ is a random force vector whose components $\eta_{i,\lambda}$ are drawn from a Gaussian distribution with zero mean and standard deviation σ defined by the correlation function $\langle \eta_{i,\lambda}(t)\eta_{i,\kappa}(t')\rangle = 2\mu^{-1}\sigma^2\delta_{\lambda\kappa}\delta(t - t')$, which ensures noise is spatially and temporally decorrelated. Collisions between the simulation box's boundaries and SPPs give rise to a force similar to the repulsion force, $\vec{F}_i^{\text{wall}} = \epsilon(1 - r_{iw}/r_0)^{3/2}\hat{r}_{iw}$, which is nonzero when the distance of the particle from the wall

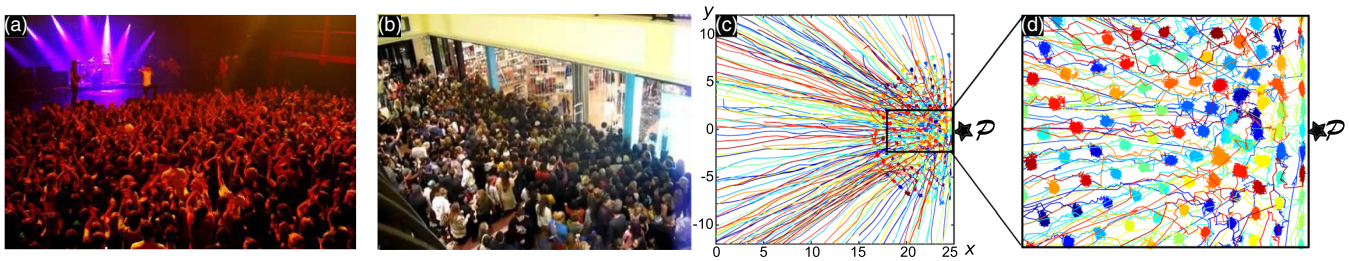

FIG. 1. Large dense groups of people give rise to emergent collective motion. (a) Attendees gather near the stage at a heavy metal concert. Credit: Ulrike Biets. (b) Customers gather for black Friday sale to purchase low-cost consumer goods. Credit: Jerry Bailey. (c) Simulated trajectories of SPPs aggregating near a point of interest $\mathcal{P}$ located at the right-most edge of a simulation box. (d) Closeup of trajectories show SPPs self-organize into a densely packed disordered aggregate.

$r_{iw} < r_0$, and is directed along the wall's outward normal direction. The functional form of $\vec{F}_i^{\text{repulsion}}$ and $\vec{F}_i^{\text{wall}}$ comes from treating SPP collisions as a Hertzian contact problem (see the Supplemental Material [18]). In terms of the simulation unit length ℓ and unit time τ, we set the particle radius $r_0 = \ell/2$, the simulation box size $L = 50\ell$, the preferred speed $v_0 = \ell/\tau$ [12], the random force standard deviation $\sigma = \ell/\tau^2$ and the force scale coefficients $\epsilon = 25\ell/\tau^2$, $\mu = \tau^{-1}$ [8]. Results presented here are for $N = 200$ SPPs, though varying population size has little effect on our analysis (see the Supplemental Material [18]).

Simulations were initialized with random initial positions for each particle. Trajectories were evolved with Newton-Stomer-Verlet integration according to $\ddot{\vec{r}}_i = \vec{F}_i^{\text{repulsion}} + \vec{F}_i^{\text{propulsion}} + \vec{F}_i^{\text{noise}} + \vec{F}_i^{\text{wall}}$ for a total of 3000τ units of time [Fig. 1(c)], where each τ consists of 10 integration time steps. While data for the initial $\approx 50\tau$ were dominated by transient motion, we discarded the first 300τ from our analysis to avoid this far-from-equilibrium effect [Fig. 1(c), linear path segments]. By 300τ the SPPs aggregated near $\mathcal{P}$ and settled into a steady-state configuration with each particle making small random motions about their average position [Fig. 1(d)]. For the model parameters studied here, collisions and random force fluctuations contribute roughly equally to these motions, as shown by comparing the relevant time scales (see the Supplemental Material [18]). At average crowd density n, the collision time scale is $\tau_{\text{coll}} = 1/(2r_0 v_0 n) \approx (\pi/4)\tau$ and the noise time scale is $\tau_{\text{noise}} = v_0^2/2\mu\sigma^2 = \tau/2$, so that $\tau_{\text{coll}} \approx \tau_{\text{noise}}$ at steady state. Thus, $\vec{F}_i^{\text{propulsion}}$ acts as an external field confining the SPPs into a disordered aggregate, while collision and noise forces drive position fluctuations within the structure [Fig. 1(d)].

Generally, we find a striking resemblance between these simulations of high-density crowds and previous studies of disordered packings [10,19–21] (see the Supplemental Material [18]). In the context of jammed granular materials, a significant amount of effort has helped develop theoretical tools that connect local structure to dynamical response [22–28]. A key analysis method involves the displacement correlation matrix whose components are defined by $C_{ij} = \langle[\vec{r}_i(t) - \langle\vec{r}_i\rangle] \cdot [\vec{r}_j(t) - \langle\vec{r}_j\rangle]\rangle$. Here, $\vec{r}_i(t)$ is the instantaneous position at time t, $\langle\vec{r}_i\rangle$ is the mean position of the ith SPP, and all averages $\langle\cdot\rangle$ are calculated by sampling position data every 10τ for a total of 270 measurements. This sampling was chosen to reduce effects of autocorrelated motion while still accumulating sufficient statistically independent measurements in a finite time [22]. In this computation, we exclude underconstrained SPPs that do not contribute to the overall collective motion. In the jamming literature these particles are called "rattlers," and they are distinguished by abnormally large position fluctuations [22]. In our analysis, we used a position fluctuation threshold of 4 standard deviations to identify rattlers. However, our results were self-consistent for values ranging from 2 to 5 indicating the methodology is robust (see the Supplemental Material [18]).

To extract quantitative information from the SPP configuration, we computed eigenmodes $\vec{e}_m$ and eigenvalues λ_m of the displacement correlation matrix. In the harmonic theory of crystals, these normal modes fully characterize the linear response of the system to perturbations [29]. For disordered materials, these modes convey information about structural stability as well as coherent and localized motion [23–25]. In nonequilibrium systems, only modes with eigenvalues that are sufficiently large play a role in determining the response to perturbations [22]. These modes must be carefully identified and interpreted due to differences between equilibrium and nonequilibrium dynamics (see the Supplemental Material [18]). Plotting the eigenvalue spectrum λ_m as a function of mode number m averaged over 10 runs with random initial conditions revealed an approximate power-law decay [Fig. 2(a), blue and orange data]. While the Debye model for 2D crystals obeys $\lambda_m \sim m^{-1}$ [Fig. 2(a), upper dashed line] [29], the simulation data has an exponent between -1 and -2. Using a random matrix model of uncorrelated Gaussian variables as a control for relevant modes [Fig. 2(a), black dotted line] (see the Supplemental Material [18]) [22], we see the lowest six eigenmodes contain information about correlated motion [Fig. 2(a), vertical black dashed line]. Plotting displacement vector fields for a few eigenmodes, we indeed find a higher degree of spatial correlation for lower m that rapidly diminishes with increasing mode number [Fig. 2(b)]. To quantify this observation, we measured the polarization of each mode's vector field and calculated the fluctuation correlation function for this

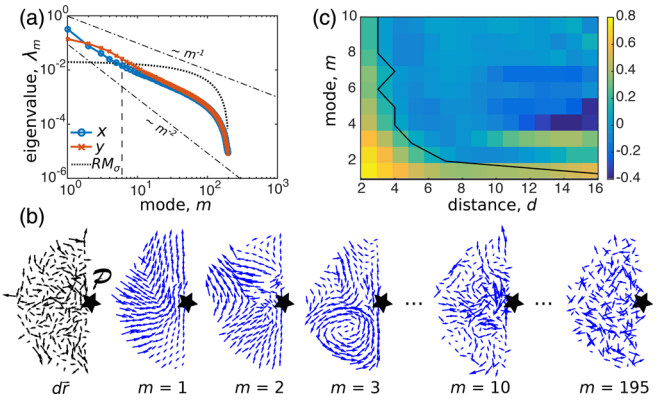

FIG. 2. Eigenmode analysis of asocial model for high-density human crowds. (a) Eigenvalue spectrum λ_m of the displacement correlation matrix exhibits scaling properties between $\lambda_m \sim m^{-1}$ and $\sim m^{-2}$ (black dashed lines). Low m eigenmodes in both x (blue) and y (orange) directions are larger than a random matrix model (RM_σ), and thus describe correlated motion. (b) Snapshot of instantaneous displacements $d\vec{r}$ and example vector fields for various eigenmodes. Lower m eigenmodes are more spatially correlated than higher m. (c) A heatmap of the polarization correlation function for the first 10 eigenmodes as a function of distance d between SPPs. Black line is where the correlation function decays to 0 demonstrating a long-range highly correlated mode for $m = 1$.

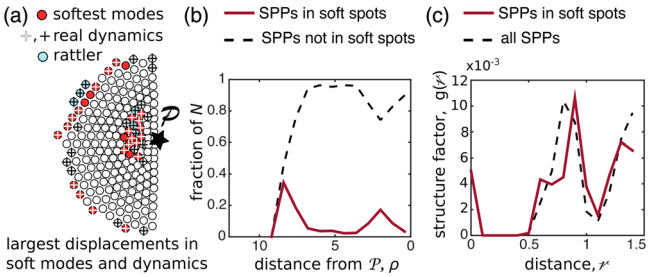

FIG. 3. Soft spots within the crowd undergo large displacements. (a) SPPs are shown as disks. Soft spots near the core of the aggregate colocalize with SPPs that displace the most in real dynamics. This region is subject to large structural rearrangements when the system is perturbed, and is likely a region where injury can occur. Apparent soft spots along the periphery are artifacts due to underconstrained edge effects. (b) Averaging over all simulation runs show soft spots generally occur near the core of the aggregate at radial distance $\rho \approx (2 \pm 1)$ away from $\mathcal{P}$. (c) Structure factor $g(r)$ measures the pair-wise SPP distribution of distances between particles and reveals structural features distinguishing SPPs in soft spots that suggest why they are subject to large displacements.

order parameter (see the Supplemental Material [18]) [30]. Remarkably, we find the first eigenmode carries a system-spanning displacement modulation [Fig. 2(c), $m = 1$], whereas the correlation for higher modes rapidly decays over a few particle diameters [Fig. 2(c), $m > 1$].

To understand the origins of this long wavelength mode, we note self-propulsion toward $\mathcal{P}$ breaks XY translational symmetry, and therefore the Goldstone theorem implies the existence of low-frequency long-wavelength deformations [31–33]. This Goldstone mode is expected to arise at low m since eigenvalues are related to vibrational frequencies by $\lambda_m = \omega_m^{-2}$, and the largest eigenvalue in the spectrum occurs at the lowest mode number [Fig. 2(a)]. Thus, the system-spanning $m = 1$ eigenmode is the system's Goldstone boson. In the context of active matter, this is known as the "Goldstone mode of the flock," and when excited, it drives the SPPs to move collectively as one [34–37]. We hypothesize a real-world example of this type of coherent long-range motion is "crowd crush" [13]. In these situations, a large number of people are suddenly displaced toward a wall, fence, or other architectural element resulting in dangerously high pressures and occasionally death [10,38]. Empirically determining if Goldstone modes are responsible for crowd crush would require careful image analysis of crowd structure and motion in the moments before such an event. Nevertheless, we expect any large dense gatherings to exhibit this type of long-range collective behavior since it originates from the general principle of symmetry breaking.

Another type of disaster found at high-density gatherings is when sudden unexpected movements of the crowd cause individuals to trip and fall. Because the majority of people are unaware this accident has happened, the rest of the crowd moves largely uninterrupted, resulting in injury or death due to trampling [10,13,39]. This is more general than the excitation of a pure Goldstone mode, and is better characterized by a superposition of modes. Thus, we focus on the particles that displace significantly more than average in a given mode m [Fig. 3(a), displacement threshold is 2.5 standard deviations more than average] (see the Supplemental Material [18]). Studies of jammed granular media show these particles, which tend to cluster in regions called "soft spots," correlate with structural rearrangements when the system is perturbed [25]. Superimposing data from the first 10 modes of a single simulation run reveals a soft spot near the core of the aggregate [Fig. 3(a)]. Regions along the perimeter also exhibit large displacements, but they are essentially underconstrained edge effects and therefore not relevant for our analysis [28]. Identifying SPPs undergoing the largest displacements in each mode up to $m = 10$ in all simulation runs show the region near the core of the crowd is the most likely area to find soft spots [Fig. 3(b), peak centered on $\rho \approx 2$]. Cross-correlating soft spot SPPs with their real-space dynamics confirmed these particles typically displace the greatest amount despite being confined within a disordered aggregate [Fig. 3(a)].

We further studied the relation between structural disorder and large displacements in soft spots by measuring the structure factor $g(r)$, which quantifies the distribution of distance r between the center of adjacent particles (Supplemental Material [18]), and found that soft spot SPPs have an intrinsically different structure compared to the average population [Fig. 3(c)]. The secondary peak in $g(r)$ around $0.5 \lesssim r \lesssim 0.8$ [Fig. 3(c) solid line] indicates soft

spot SPPs are more highly squeezed by some of their neighbors, while the shifted peak centered on $r \approx 0.9$ indicates they are also further away than average from other neighbors [Fig. 3(c), dashed line peak at $r \approx 0.8$]. These data suggest soft spot SPPs are being compressed tightly in one direction, and as a consequence displace greater amounts in the orthogonal direction. As such, self-organized structural disorder is fundamental for large displacements and rearrangements [Fig. 3(a)] [25]. Because these large random rearrangements would likely be experienced as unexpected lurching movement for the average member of a human crowd, we hypothesize soft spots pose the greatest risk for tripping and subsequent trampling. If found true, real-time image analysis identifying soft spots in densely packed human crowds may provide useful predictive power for preventing injuries.

Our results thus far have focused on structural origins of collective motion with all model parameters kept constant. In real life situations, not all people behave the same: some agitate more easily, others less so [9,15]. Accordingly, we modify the asocial model to study how mechanisms for coherent collective motion are affected by active perturbations. Specifically, we introduce a second population of SPPs so that a fraction f exhibits a more agitated behavior, while the remaining fraction $1 - f$ of the population is the same as before [8,9]. We model these agitated SPPs with a larger distribution of force fluctuations in $\vec{F}_i^{\text{noise}}$ by increasing their standard deviation to $\sigma_a > \sigma$, and analyze the two parameter phase space of f and σ_a. We first consider the case $\sigma_a = 3\sigma$ and vary f from 0 to 1. Calculating the spectrum of eigenvalues λ_m shows the qualitative trends are independent of f, though numerical values of λ_m tend to increase with more agitators (see the Supplemental Material [18]). To understand how long-range collective motion is affected by agitated SPPs, we measured the polarization fluctuation correlation function for the first 10 modes while varying σ_a and f [Fig. 4]. Surprisingly, the correlation functions for $\sigma_a = 3\sigma$ show a qualitative transition with varying f unanticipated from the eigenvalue spectrum: the eigenvalues smoothly vary with mode number while the correlation functions exhibit new behaviors. For $f = 0.1$, a long-range correlated Goldstone mode is observed as before. However, multiple long-range correlated modes are observed for $f = 0.2$, and no long-range correlated modes are observed for $f > 0.3$. Examining other values of σ_a shows a similar transition with increasing f from a single well-defined long-range mode, to multiple long-range modes, to no long-range modes whatsoever [Fig. 4, along rows, read left-to-right].

The low-agitation and high-agitation limits are intuitive. For low agitation [Fig. 4, white region], additional force fluctuations through increasing σ_a with low f or increasing f with low σ_a induce small perturbations to the overall structure. As such, the existence of a Goldstone mode at low m is anticipated based on the homogeneous population results [Fig. 2(c)]. For high agitation where the combined effect of σ_a and f is large [Fig. 4, dark gray shaded region], we expect local structure to break down and correlated

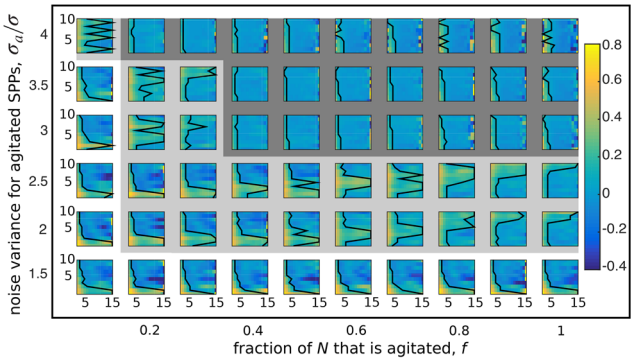

FIG. 4. Introducing a fraction f of agitated SPPs with variance σ_a in $\vec{F}_i^{\text{noise}}$ probes structural origins of collective motion. Each heat map is the polarization fluctuation correlation function for the first 10 eigenmodes as a function of distance d [same as Fig. 2(c)]. Low fluctuations (white background) preserve the long-range highly correlated Goldstone mode near $m = 1$. High fluctuations (dark gray background) destroy long-range correlated modes. Intermediate fluctuations (light gray background) add new modes with long-range correlations, indicating stochastic resonance.

motion to be marginalized. Consistent with this reasoning, we find no long-range modes in the high-agitation limit.

Between the high and low agitation limit, we find a boundary in the (f, σ_a) phase diagram characterized by multiple long-range modes [Fig. 4, light gray shaded region]. This result is striking because it shows moderate levels of noise produce new coherent motion. Noting that correlated motion allows mechanical information to be transferred across the aggregate, an appearance of multiple long-range modes implies greater information bandwidth. In certain settings, signal enhancement mediated by noise is called *stochastic resonance* [40,41]. Generally, stochastic resonance is found in systems where nonlinear effects dampening signal propagation are suppressed by random noise. In our case, nonlinear effects suppressing conventional phonon modes come from structural packing disorder. Random noise from agitators increases the internal pressure within the aggregate, breaking up the disordered configuration of particle-particle contacts. Consequently, phonon modes otherwise suppressed by packing disorder [Fig. 2(c), modes $m > 1$] reassert their presence [Fig. 4, additional long-range modes in light-gray region] (see the Supplemental Material [18]). In the context of our model, this indicates that modest random fluctuations can enhance overall collective motion, increasing the potential for injurious outcomes in high-density crowds.

Our analysis of collective motion in dense crowd simulations relies on trajectory data in order to identify and understand the emergence of Goldstone modes, soft spots, and stochastic resonance. With an eye to crowd safety, the dependence on measurable quantities combined with computer vision techniques [42,43] provides significant potential for applications in real-time crowd management, which may help protect attendees at large gatherings by reducing

emergent risks [10,15,39]. More theoretically, the observation of Goldstone modes hints at a collective motion analogous to the Higgs boson that may be found in collective speed modulations. To elaborate, active matter systems breaking continuous rotational symmetry can be represented by an orientation field quantifying the SPP vector headings. Long-range fluctuations in orientation correspond to the zero-energy Goldstone mode. Associated with this velocity vector *orientation* field is the velocity vector *speed* field. This speed field is subject to fluctuations with an energetic cost that does not go to zero at infinite wavelength, indicating the presence of a massive boson otherwise known as the Higgs boson. Developing an effective field theory around these ideas and incorporating quasiparticlelike excitations would likely present new opportunities for understanding emergent collective motions, their interactions, and potential hazards in large social gatherings.

We thank U. Biets and J. Bailey for providing photographs used here. A. B. thanks A. Maffini for discussions during the early stages of the project. J. L. S. thanks M. Bierbaum, J. Sethna, and I. Cohen for useful discussions. Thanks to A. Gådin and J. Svensson for software development. A. B. acknowledges funding from the Centre for Interdisciplinary Mathematics (CIM). J. L. S. was independently funded.

*arianna.bottinelli@math.uu.se
†david.sumpter@math.uu.se
‡jesse.silverberg@wyss.harvard.edu

[1] S. Camazine, *Self-Organization in Biological Systems* (Princeton University Press, Princeton, NJ, 2003).
[2] D. J. Sumpter, *Collective Animal Behavior* (Princeton University Press, Princeton, NJ, 2010).
[3] T. Vicsek and A. Zafeiris, Phys. Rep. **517**, 71 (2012).
[4] D. Helbing and P. Molnar, Phys. Rev. E **51**, 4282 (1995).
[5] D. Helbing and A. Johansson, *Pedestrian, Crowd and Evacuation Dynamics* (Springer, New York, 2011).
[6] H. Xi, S. Lee, and Y.-J. Son, in *Human-in-the-Loop Simulations* (Springer, New York, 2011), pp. 69–95.
[7] M. Moussaïd, D. Helbing, and G. Theraulaz, Proc. Natl. Acad. Sci. U.S.A. **108**, 6884 (2011).
[8] J. L. Silverberg, M. Bierbaum, J. P. Sethna, and I. Cohen, Phys. Rev. Lett. **110**, 228701 (2013).
[9] D. Helbing, I. J. Farkas, and T. Vicsek, Phys. Rev. Lett. **84**, 1240 (2000).
[10] D. Helbing, A. Johansson, and H. Z. Al-Abideen, Phys. Rev. E **75**, 046109 (2007).
[11] D. C. Duives, W. Daamen, and S. P. Hoogendoorn, Transport. Res. C—Emer. **37**, 193 (2013).
[12] D. Helbing, I. Farkas, and T. Vicsek, Nature (London) **407**, 487 (2000).
[13] J. J. Fruin, Eng. Crowd Safety **1**, 10 (1993).
[14] K. M. Zeitz, H. M. Tan, M. Grief, P. Couns, and C. J. Zeitz, Preshosp. Dis. Med. **24**, 32 (2009).
[15] E. A. Heide, in *The First 72 hours: A Community Approach to Disaster Preparedness*, edited by M. O'Leary (iUniverse, Lincoln, NE, 2004), p. 337.
[16] T. Janchar, C. Samaddar, and D. Milzman, Am. J. Emerg. Med. **18**, 62 (2000).
[17] J. Bohannon, Science **310**, 219 (2005).
[18] See Supplemental Material at http://link.aps.org/supplemental/10.1103/PhysRevLett.117.228301 for additional methods, results, and analysis.
[19] D. Helbing, A. Johansson, J. Mathiesen, M. H. Jensen, and A. Hansen, Phys. Rev. Lett. **97**, 168001 (2006).
[20] E. Cristiani, B. Piccoli, and A. Tosin, Multiscale Model. Sim. **9**, 155 (2011).
[21] S. Faure and B. Maury, Math. Models Methods Appl. Sci. **25**, 463 (2015).
[22] S. Henkes, C. Brito, and O. Dauchot, Soft Matter **8**, 6092 (2012).
[23] C. Brito, O. Dauchot, G. Biroli, and J.-P. Bouchaud, Soft Matter **6**, 3013 (2010).
[24] D. J. Ashton and J. P. Garrahan, Eur. Phys. J. E **30**, 303 (2009).
[25] M. L. Manning and A. J. Liu, Phys. Rev. Lett. **107**, 108302 (2011).
[26] S. Henkes, Y. Fily, and M. C. Marchetti, Phys. Rev. E **84**, 040301 (2011).
[27] N. Xu, V. Vitelli, A. Liu, and S. Nagel, Europhys. Lett. **90**, 56001 (2010).
[28] P. Charbonneau, E. I. Corwin, G. Parisi, and F. Zamponi, Phys. Rev. Lett. **114**, 125504 (2015).
[29] N. W. Ashcroft and N. D. Mermin, *Solid State Physics* (Thomson Learning, San Diego, CA, 1976), p. 120.
[30] W. Bialek, A. Cavagna, I. Giardina, T. Mora, O. Pohl, E. Silvestri, M. Viale, and A. M. Walczak, Proc. Natl. Acad. Sci. U.S.A. **111**, 7212 (2014).
[31] Y. Nambu, Phys. Rev. **117**, 648 (1960).
[32] J. Goldstone, Il Nuovo Cimento **19**, 154 (1961).
[33] J. Sethna, *Statistical Mechanics: Entropy, Order Parameters, and Complexity* (Oxford University Press, Oxford, England, 2006).
[34] J. Toner, Y. Tu, and S. Ramaswamy, Ann. Phys. (Amsterdam) **318**, 170 (2005).
[35] S. Ramaswamy, Annu. Rev. Condens. Matter Phys. **1**, 323 (2010).
[36] A. Cavagna, A. Cimarelli, I. Giardina, G. Parisi, R. Santagati, F. Stefanini, and M. Viale, Proc. Natl. Acad. Sci. U.S.A. **107**, 11865 (2010).
[37] W. Bialek, A. Cavagna, I. Giardina, T. Mora, O. Pohl, E. Silvestri, M. Viale, and A. M. Walczak, Proc. Natl. Acad. Sci. U.S.A. **111**, 7212 (2014).
[38] S. C. Takatori, W. Yan, and J. F. Brady, Phys. Rev. Lett. **113**, 028103 (2014).
[39] B. Krausz and C. Bauckhage, Computer Vision and Image Understanding **116**, 307 (2012).
[40] M. D. McDonnell and D. Abbott, PLoS Comput. Biol. **5**, e1000348 (2009).
[41] L. Gammaitoni, P. Hänggi, P. Jung, and F. Marchesoni, Rev. Mod. Phys. **70**, 223 (1998).
[42] J. S. J. Junior, S. Musse, and C. Jung, IEEE Signal Process. Mag. **5**, 66 (2010).
[43] S. Ali, K. Nishino, D. Manocha, and M. Shah, *Modeling, Simulation and Visual Analysis of Crowds: A Multidisciplinary Perspective* (Springer, New York, 2013).